International Journal of Automotive Research, Vol. 10, No. 3, (2020), 3281-3294

Iran University of Science and Technology

International Journal of Automotive Engineering

Journal Homepage: ijae.iust.ac.ir

ISSN: 2008-9899

Experimental study and thermal analysis of a Gamma type Stirling engine for multi-objective optimization

Mohammad Reza Azmoodeh[1], Ali Keshavarz[2*], Alireza Batooei[3] , Hojjat Saberinejad[3] , Mohammad Payandehdoost[1] , Hossein Keshtkar[1]

[1] PhD Student, Department of Mechanical Engineering, K.N. Toosi University of Technology, Tehran, Iran.

[2] Professor, Department of Mechanical Engineering, K.N. Toosi University of Technology, Tehran, Iran.

[3] PhD, Department of Mechanical Engineering, K.N. Toosi University of Technology, Tehran, Iran.

ARTICLE INFO

Article history:

Received: 20 July 2020

Accepted: 10 Aug 2020

Published:1 Sep 2020

Keywords: Stirling engine, Experimental study, Numerical analysis, Thermal balance, multi-objective optimization, efficiency, DOE method

A B S T R A C T

A multi-objective optimization and thermal analysis is performed by both experimental and numerical approaches on a Stirling engine cooler and heater. The power generated is measured experimentally by an electrical engine coupled with the crank case, and the friction is estimated by the difference between the necessary power used for rotating the engine at a specific pressure and speed, versus the actual power measured experimentally. In the experimental approach, different conditions were considered; for example, the charge pressure varied from 5-9 bars, and the engine speed varied from 286-1146 rpm. The maximum power generated was 461.3 W and was reported at 9 bars of charge pressure and 1146 rpm engine speed. Numerical approach was carried to simulate thermal balance for investigations on the effect of friction, engine speed and efficiency on generated engine power. Average values of Nusselt number and coefficient of friction were suggested from simulation results.

The multi-objective optimization was held using DOE method for maximizing engine efficiency and power, and also minimizing pressure drop. The top and bottom boundary values for our optimization were 5-9 bars of pressure and 286-1146 rpm of engine speed; for both helium and carbon dioxide. To do so, all three significance factors (engine speed, efficiency and friction) were given different weights, thus different combinations of weight value was investigated

Amongst different interesting findings, results showed that if the efficiency weight factor changed from 1 to 3, for helium in a specific condition, the optimum engine speed would increase by approximately 30.6 %

1. Introduction

Stirling engines are external combustion engines which in theory have a promising thermodynamic efficiency. These engines can be operated using a variety of fuels, making them environmentally friendly and also their flexibility in fuel offers a variety of options including sustainable energy sources. Thus in recent years, Stirling engines have attracted the attention of many researchers.

*Corresponding Author
Email Address: keshavarz@kntu.ac.ir
https://doi.org/10.22068/ase.2020.547

[DOI: 10.22068/ase.2020.547]

Karabulut et al. conducted experiments on an β-Stirling engine using helium as the operating fluid, and LPG as fuel source. It was shown that the engine initially starts rotating at about 118℃. Experiments where conducted at heating temperatures of 180℃, 220℃ and 260℃, whilst charging pressure varied from 1 to 4 bars. The results showed the maximum output torque of 3.99 N.m along with a maximum power of 183W was achieved at charge pressure of 4bars and heating temperature of 260℃. [1]

Cheng et al. prepared a computational model to investigate the influence of rotational speed on the output power of the Stirling engine. The variation of expansion and compression chamber temperature is related to engine speed. These temperatures are computed by using Lumped-mass model in presented model. The results showed that increment of rotational speed and temperature difference between compression and expansion chamber reduces leads to decrease the output power. The power is increased to a maximum value by increasing the rotational speed, and then reduces again. [2]

Toghyani conducted third-order thermodynamic analysis from multi-objective optimization of a GPU-3 stirling engine. In their optimizations, four variables namely, heating temperature, piston stroke, effective pressure and engine frequency were investigated. They used multi-objective techniques such as Epsilon-Constrained method and the weighted sum method, with the aim of achieving best efficiency, best power and minimum pressure loss. [3]

Ahmadi et al. analyzed the optimization of thermal efficiency, engine power and pressure drops using NSGA algorithm. In that study, eleven variables were chosen and their range of changes were defined. Decision making methods of TOPSIS, LINMAP and FUZZY Bellman-Zadeh were used. Correlations were suggested to predict efficiency in pressure terms. [4]

Alfarawi et al. developed a non-ideal adiabatic thermodynamic model for a γ-Stirling engine. They supported their model by experimental measurements showing a maximum deviation between simulation and experimental results were 16.9%. simulation results showed that if we reduced the coolant temperature from 15℃ to -50℃ while maintaining heat source at 650℃; we could increase the generated power by 49% if running on helium, or by 35% if running on nitrogen. [5]

Saberinejad et al. analyzed thermodynamic cycle of a Stirling engine by employing a new analytical model. They evaluated the output power and efficiency of real Stirling engines by applying correcting functions on the Schmidt equations to achieve more accurate results with respect to the adiabatic model. The comparison indicates that the model results are in good agreement with the available output data of GPU-3 Stirling engine output. [6]

Ye et al. study and optimize the performance of a free piston Stirling engine by response surface methodology (RSM) and the desirability approach and found that free piston SE's parameters which have a significant e□ect on the output power and thermal e□ciency. They found these increase with the charge pressure, operating frequency, and hot end temperature, while they decrease with the rise of the cooler length. [7]

Ahmed et al. developed a practically feasible thermodynamic model for beta type of Stirling engines with rhombic-drive mechanism. The optimized model was later compared with the various experimental data of GPU-3 and Substantial improvement on the performance of the engine is achieved by optimizing the operating and geometric parameters of the beta type stirling engine. [8]

In this research we experimentally investigated a γ-type Stirling engine built by IPCO, using helium as working fluid. From the experiments, the engine output heat, power output, heats absorbed by the engine and friction losses were measured. The temperature of water into and out of the cooler were measured, along with surface temperature of the hot-end heat exchanger. To further investigate the input and output heat of the engine, numerical simulation of the cold and hot heat exchangers was studied. Also the effects of charge pressure and rotational speed on the exchanged, heat in and out of the engine, were investigated. And a correlation to obtain the Nusselt number along with the coefficient of friction is proposed. By comparing simulation data against actual experimental data, the biggest deviation was 9.4%, showing sufficient accuracy in simulation results.

Finally, multi-objective optimization is done by DOE method on this engine to novelty an optimum point of working pressure and rotational speed of the engine to maximize the efficiency and power and minimize the pressure for helium and carbon dioxide as working fluid.

[DOI: 10.22068/ase.2020.547]

2. Experimental investigations of the ST-500 Stirling engine

In table 1 we can see the geometry and operation parameters of the ST500 engine. All experimental work on this engine has been held in the Stirling Research Center and IPCO [9].

Table 1: Specifications of the ST500 Stirling engine

Specification	Values
Type	Gamma
Electrical output power	461 W
Total efficiency	8.2 %
Standard charge pressure	9 bar
Working fluid	He , CO_2
Working frequency	19.1 Hz
Fuel	Natural gas
Cooling substance	Water
Power piston stroke	75 mm
Power piston diameter	84 mm
Displacer stroke	75 mm
Displacer diameter	97 mm
Clearance Volume	804000 mm^3
Phase angle	90 ◦
Heater type	Tublar (6mm dia.) *20
Regenerator material	Steel matrix (0.96 porosity)
Heat absorbtion temperature	350-420 ℃
Heat rejection temperature	30-50 ℃

A photo from the engine is shown in fig.1 with four temperature sensors and one pressure sensor labeled in fig. 1. The temperature sensors are listed in Table 2, measure the input/output water temperature to-and-from the cooler; along with two sensors on the hot-end heat exchanger's surface. A pressure sensor is fitted to measure charge pressure and control pressure fluctuations. The ST-500 is fitted with a one-way valve for charging the working fluid into the engine, this valve prevents the charged fluid from discharging.

Table 2: Measuring items and position of measuring point

Object	Position	Measuring instrument
Temperature	Inlet water to cooler	K-Type thermocouple
Temperature	Outlet water from cooler	K-Type thermocouple
Temperature	Outer wall of heater tubes	K-Type thermocouple
Temperature	Outer wall of heater tubes	K-Type thermocouple
Pressure	The body of Engine	Pressure transducer

The nine serials of tests are performed for considering the fluid behavior at various pressure and rotational speed. These results are used for simulation validation and to support the analysis results.

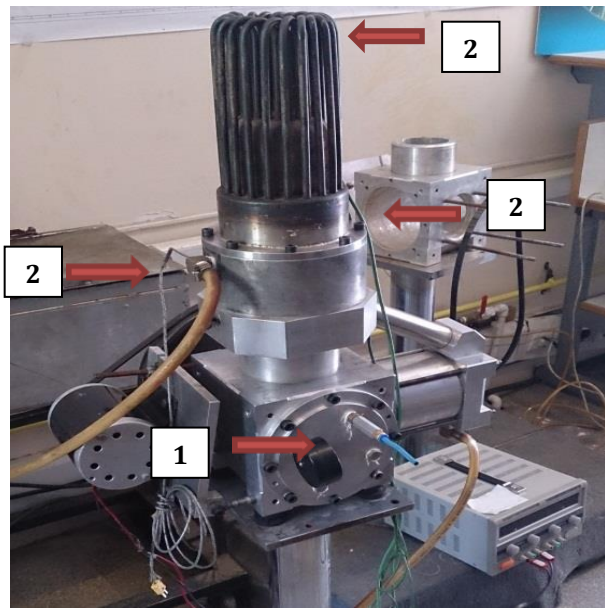

Figure 1: Experiment setup of the ST500 Stirling Engine and placement of pressure sensors (No.1) and temperature sensors (No.2)

As we know, the efficiency of a Stirling engine can be calculated via eq.1

$$\eta = \frac{W}{Q_h} \quad (1)$$

The extracted heat from the cold-end heat exchanger can easily be measured by reading the two heat sensors at both ends of the heat exchanger and calculating eq.2 considering water flow.

$$\dot{Q}_l = \dot{m} C_P (T_1 - T_2) \quad (2)$$

T_1 is the temperature of cold water entering the cooler, and T_2 is the elevated water temperature exiting the engine. The power generated can also be calculated by eq.3 using the generated voltage and current inside the A.C invertor. With regard to eq.3, cosØ=0.746 for the three-phase engine.

$$W = \sqrt{3}.V.I.\cos\varphi \quad (3)$$

Thus using eq.4 we can calculate the total input thermal energy from the first law of thermodynamics.

$$W = Q_h - Q_l \quad (4)$$

Friction can be measured by reversing the generator connected to the engine. This way one can easily calculate the difference between electrical power input and the output mechanical power.

In table 3, we showed experimental values of input energy, extracted thermal energy, friction and generated power; all whilst operating between 3 to 9 bars of helium as working fluid, and 30 to 120 rad/s rotational speed.

[DOI: 10.22068/ase.2020.547]

3. Numerical analysis of heat exchangers of the ST-500

The shape and specification of the heat exchangers can be seen in fig.2 and table 4. Simulation of both heat exchangers have been achieved within pressure range of 3-9 bars and rotational speeds of 286-1146 rpm for both helium and carbon dioxide a working fluids. The cooler assumed to be adiabatic.

In situations where we have compressible flow, thus density is a variable, a mean-weighted time-average method is used to represent the flow. This method is also knowing as Favre-Average method [10]. so the governing equation would be as follows:

Continuity equation:

$$\frac{\partial \bar{\rho}}{\partial t}+\frac{\partial}{\partial x_i}(\bar{\rho}\tilde{u}_i)=0 \quad (5)$$

Momentum equation:

$$\frac{\partial}{\partial t}(\bar{\rho}\tilde{u}_i)+\frac{\partial}{\partial x_j}(\bar{\rho}\tilde{u}_i\tilde{u}_j) = -\frac{\partial P}{\partial x_i}+\frac{\partial}{\partial x_j}(\bar{\tau}_{ij}-\overline{\rho u_i'' u_j''}) \quad (6)$$

Energy equation: (7)

$$\frac{\partial}{\partial t}\left[\bar{\rho}\left(\tilde{e}+\frac{\tilde{u}_i\tilde{u}_i}{2}\right)+\frac{\overline{\rho u_i'' u_i''}}{2}\right] + \frac{\partial}{\partial x_j}\left[\bar{\rho}\tilde{u}_j\left(\tilde{h}+\frac{\tilde{u}_i\tilde{u}_i}{2}\right)+\tilde{u}_j\frac{\overline{\rho u_i'' u_i''}}{2}\right] = \frac{\partial}{\partial x_j}\left[-q_{Lj}-\overline{\rho u_j'' h''}+\bar{\tau}_{ji}u_i'' - \overline{\rho u_j''\frac{1}{2}u_i'' u_i''}\right] + \frac{\partial}{\partial x_j}\left[\tilde{u}_i+(\bar{\tau}_{ij}-\overline{\rho u_i'' u_j''})\right]$$

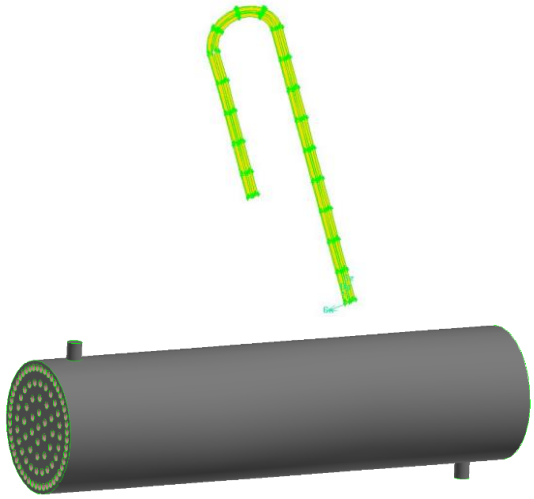

Figure 2: Geometry of heater (up) and cooler (down)

Table 4: Specifications of the heat exchangers

Specification	Values
Heater	
Tube diameter	6 mm
Curvature of Heater diameter	16 mm
Length of small tube	90 mm
Length of large tube	180 mm
Cooler	
Tube diameter	4 mm
Shell diameter	107 mm
Length of shell and tube	240 mm
Number of tubes	91

For Newtonian fluids, τ_{ji} is defined as Eq.(8).

$$\tau_{ji}=2\mu s_{ij}+\zeta\frac{\partial u_k}{\partial x_k}\delta_{ij} \quad (8)$$

$$s_{ij}=\frac{1}{2}\left(\frac{\partial u_i}{\partial x_j}+\frac{\partial u_j}{\partial x_i}\right) \quad (9)$$

Table 3: Generated power, friction work, heating and cooling loads at different charge pressure's and engine speeds

Item	Pressure (bar)	Engine speed (r.p.m)	Cooling load (W)	Heating load (W)	Friction(W)	Work (W)
1	5	286	161.4	1057.9	814	82.5
2	5	573	351.7	1930.7	1454.3	124.7
3	5	858	557.1	2670.2	1991.8	121.3
4	5	1146	772.7	3292.5	2452	67.8
5	9	286	344.8	1770	1228.1	197.1
6	9	573	751.9	3157.3	2069.9	335.5
7	9	858	1182.7	4447.7	2845.9	419.1
8	9	1146	1627.6	5636.2	3547.3	461.3

[DOI: 10.22068/ase.2020.547]

Where, μ is dynamic viscosity which correlates the tension and liner deformation and ζ correlates the tension and volumetric deformation.

The approximated magnitude for volumetric deformation is calculated from Eq. (10). [11]

$$\zeta = -\frac{2}{3}\mu \tag{10}$$

In this research the viscosity is computed from Sutherland law [12].

$$\mu = \mu_0 \left(\frac{T_0 + T_{su}}{T + T_{su}}\right)\left(\frac{T}{T_o}\right)^{\frac{3}{2}} \tag{11}$$

Where, μ_0 is reference value of viscosity, T_0 is reference value of temperature, T_{su} is Sutherland constant for gas and T is the gas temperature. The heat flux vector is computed by Eq. (12).

$$q_j = -k\frac{\partial T}{\partial x_j} \tag{12}$$

It should be noted the thermal conductivity (k) is calculated at mean temperature. Also the specific energy and enthalpy are defined as Eq. (13) and (14).

$$e = C_v T \tag{13}$$

$$h = C_P T \tag{14}$$

The ideal gas assumption results C_v and C_P be constant. By defining dimensionless parameters as $u^* = \frac{u}{u_{max}}$, $x^* = \frac{x}{D}$, $P^* = \frac{P}{\rho_o {u_{max}}^2}$, $\rho^* = \frac{\rho}{\rho_0}$ and $t^* = t\omega$, the momentum equation would be reached as equation 15.

$$\frac{\partial}{\partial t^*}(\overline{\rho^* \widetilde{u^*}_i}) + \frac{A_0}{2}\frac{\partial}{\partial x_j^*}(\overline{\rho^* \widetilde{u^*}_i \widetilde{u^*}_j}) = -\frac{A_0}{2}\frac{\partial P^*}{\partial x_i^*} + \frac{1}{Re_\omega}\frac{\partial}{\partial x_j^*}\left[\left(\frac{\partial u_j^*}{\partial x_i^*} + \frac{\partial u_i^*}{\partial x_j^*}\right) - \frac{2}{3}\frac{\partial u_k^*}{\partial x_k^*}\right]\delta_{ij} - \frac{A_0}{2}\frac{\partial}{\partial x_j^*}(\overline{\rho^* {u''}_i^* {u''}_j^*}) \tag{15}$$

Where $A_0(\frac{x_{max}}{D})$ and $Re_\omega(\frac{\rho\omega D^2}{\mu})$ are dimensionless flow displacement and kinetic Reynolds number, respectively.

The $k-\varepsilon$ model is performed to analyzing turbulence in flow duo to previous researches. [12, 13, 14]

The numerical simulation is performed using finite volume approach and pressure-based method. The time constant used in this research is defined by Eq. 16 and its minimum order is about -2. So the time step should be at least in order of -3.

$$T = \frac{2\pi}{\omega} \tag{16}$$

In order to select the most suitable time step, three different steps were investigated ($\frac{T}{9}, \frac{T}{90}, \frac{T}{900}$). As a reference point, we measured the temperature at mid-section of hot-end heat exchanger. Results showed the difference between $\frac{T}{90}$ and $\frac{T}{900}$ time steps was less than 0.433%, proving $\frac{T}{90}$ is an adequate time step.

Also to investigate mesh independency, the Nusselt number inside the heater was calculated using four mesh sizes (280,000/350,000/420,000/500,000 meshes). As can be seen from fig.3, the two cases with 420,000 and 500,000 meshes was chosen suitable for simulation purposes.

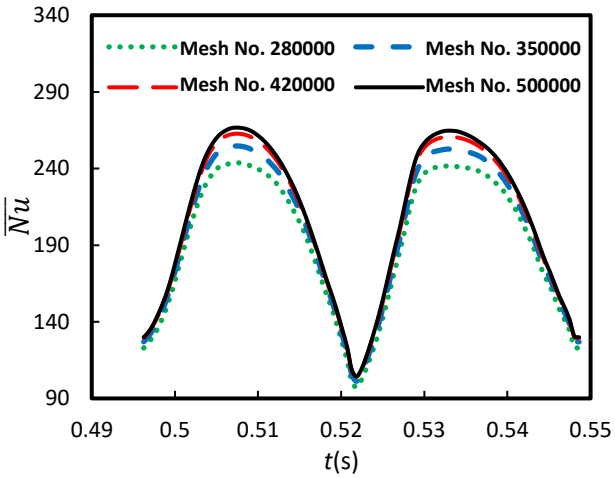

Figure 3: investigating mesh independency considering Nusselt number

The engine boundary conditions were set the same as had been measured from experimental investigations. Also a simple function was applied on the velocity term to take account for the speed fluctuations and direction changes eq.17. [15]

$$u = \left(\frac{{d_P}^2}{n\,{d_{in}}^2}\right)\left(\frac{2SN_r}{60}\right) \tag{17}$$

To verify the results, we compared the cyclic average coefficient of friction from our calculations to those found from experimental data and the findings of Zhao & Cheng [15],

*Corresponding Author
Email Address: keshavarz@kntu.ac.ir
http:// tlx.doi.org/10.22068/ijae.10.3.3281

[DOI: 10.22068/ase.2020.547]

Table 5: boundary conditions for input and output velocity of hot end heat exchange

Item	Engine Speed (r.p.m)	Velocity (m/s)
1	286	$\pm 9.17 \sin 30t$
2	572	$\pm 18.34 \sin 60t$
3	859	$\pm 27.51 \sin 90t$
4	1146	$\pm 36.68 \sin 120t$

in which they investigated the coefficient of friction for different kinetic Reynolds numbers and frequencies of a turbulent flow in a straight pipe of 1.35 cm diameter and length-to-diameter ratio of 70. Eq. 18:

$$\bar{C}_{f,t} = \frac{1}{A_0}\left(\frac{76.6}{Re_\omega^{1.2}} + 0.40624\right) \qquad (18)$$

$$81 \leq Re_\omega \leq 540 \ \& \ 53.4 \leq A_0 \leq 113.5$$

Zhao & Cheng [16] also investigated the coefficient of friction in a laminar reciprocating flow. Eq. 19:

$$\bar{C}_{f,l} = \frac{3.27192}{A_0(Re_\omega^{0.548} + 2.03946)} \qquad (19)$$

$$23 \leq Re_\omega \leq 395 \ \& \ 0 \leq A_0 \leq 26.4$$

Our results was compared to Zhao & Cheng's findings in fig.4, showing reasonable accuracy, and a deviation of 10.5% at the most which occurred when $Re_\omega = 400$ and $A_0 = 66.8$.

Regarding previous research on Nusselt number correlations, we point out to Dittus-Boelter's correlation for stable turbulent flow [17].

$$\mathrm{Nu} = 0.023\mathrm{Re}^{0.8} Pr^{0.4}\left(T_w/T_g\right)^{-0.5} \qquad (20)$$

$$10^4 \leq Re \leq 1.2 \times 10^5$$

$$0.7 \leq Pr \leq 120 \ \& \ ; \frac{L}{D} \geq 60$$

Kanzaka-Lwabuchi conducted experimental research on the phase difference of engine pistons according to the Schmit model, based on Dittus-Boelters equation. They recommended finding Nusselt number from eq.21 [18].

$$\mathrm{Nu} = 0.023\mathrm{Re}^{0.8} Pr^{0.4}\left(T_w/T_g\right)^{-0.5} \ C \qquad (21)$$

$$\mathrm{C} = 0.923 + 0.75(T_w/1000)$$

$$10^4 \leq Re \leq 1.2 \times 10^5$$

$$0.7 \leq Pr \leq 120 \ \& \ ; \frac{L}{D} \geq 60$$

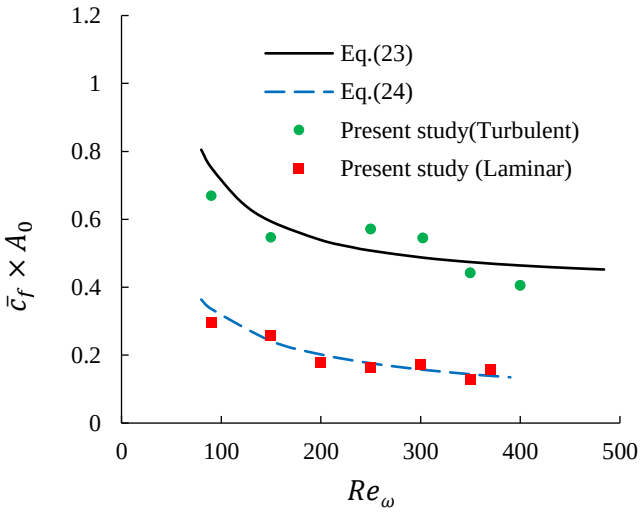

Figure 4: verification of numerical results

Zhao & Cheng proposed a correlation for Nusselt number in a straight pipe containing laminar flow in equation below. [19]

$$\mathrm{Nu} = 0.02{\mathrm{Re}_w}^{0.58}{A_0}^{0.85} \qquad (22)$$

$$0 < Re_w < 500 \quad ; \ A_0 = 8.5; 15.3; 20.4; 34.9$$

In this research, we compared our results on the Nusselt number with those of Dittus-Boelter, Kanzaka-Lwabuchi and Zhao-Cheng's findings.

To have a fair comparison, it's required to maintain same geometry for cases being compared. Since no experimental data exists for heat transfer in a compressible turbulent reciprocating flow in a U-tube in the dimensionless range discussed in this paper; we had to compare experimental data with:
a) uni-direction flow in a strait pipe.
b) uni-direction turbulent flow in a U-tube.
c) Reciprocating laminar flow in a U-tube.

The results of the comparison are shown in fig. 5. It's pointed out that the Zhao-Cheng correlation exists for laminar reciprocating flow in a pipe, thus their results regarding heat transfer is expected to be smaller than those found in this research since we considered the flow to be turbulent.

In the case of Kanzaka-Lwabuchi, heat transfer was reported higher than those found in this research at high Reynolds numbers, due to the fact that their Arc-shaped geometry was different from our U-tubes. Similar numerical solution was used for the cooler heat exchanger of the engine.

[DOI: 10.22068/ase.2020.547]

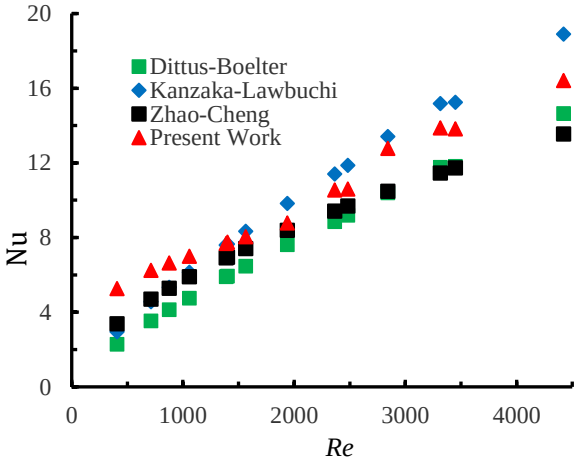

Figure 5: comparison if Nusselt number variation against maximum Reynolds number of current study versus uniform turbulent flow in a straight pipe (Dittus-Boelter), uniform turbulent flow in arc-shape pipe (Kanzaka-Lawbuchi), and laminar reciprocating flow (Zhao-Cheng).

4. Multi-objective optimization by Design of Experiment (DOE) method

The multi-objective optimization is performed by using DOE method. Many researchers have considered two or more parameters in their investigations, in this research we considered a two-level factorial design with operational pressure and rotational speed as selected parameters. In order to do so, four experimental-or-simulation set of results was required for a detailed investigation. For each parameter, we needed to define the maximum/minimum values; so for operational pressure we presumed it to be between 3-9 bars, and for rotational speed we presumed 286-1146 rpm. We also defined our main investigation scope to be output power, efficiency and pressure drop.

If we aimed to maximize a target, then eq.23 is held:

$$d_i = 0 \qquad y_i < L_i \qquad (23)$$

$$d_i = ((y_i - L_i)/(T_i - L_i))^{r_i} \qquad L_i \le y_i \le T_i$$

$$d_i = 1 \qquad y_i > T_i$$

Where, y_i , L_i, T_i and r_i are predicted value of i_{th} response, lowest acceptable value for i_{th} response, target value for i_{th} response and weight of desirability function of i_{th} response, respectively.

$$d_i = 0 \qquad y_i > U_i \qquad (24)$$

$$d_i = ((U_i - y_i)/(U_i - T_i))^{r_i} \qquad T_i \le y_i \le U_i$$

$$d_i = ((U_i - y_i)/(U_i - T_i))^{r_i} \qquad T_i \le y_i \le U_i$$

Where, U_i is highest acceptable value for i_{th} response. The combined desirability is calculated by Eq (۲۵).

$$D = \left(\sum (d_i^{wi})\right)^{1/W} \qquad (25)$$

$$W = \sum w_i \qquad (26)$$

The weight coefficient indicates how to reach the target function, for each individual target. For each target, the weight coefficient varies from 0.1-10 to specify the importance of the selected target.
- If the weight coefficient is between 1 and 0.1: Little importance exists on the target effect.
- If the weight coefficient is 1: Target effect has the same importance as other function boundaries
- If the weight coefficient is between 1 and 10: Significant importance exists on reaching the target effect.

5. Optimization Results and discussion

According to simulation results for both cooler and heater section of the Stirling ST500 engine, correlations are suggested for average Nusselt number and average coefficient of friction in the heater for carbon dioxide and helium as working fluids, in dimensionless terms of Prandtl and kinetic Reynolds numbers.

The average Nusselt number for carbon dioxide and helium can be found from eq. ۲۷-۲۸ knowing the average Nusselt number in the heater along with coefficient of heat convection, the heat transferred to the heater can be calculated.

$$\overline{Nu} = 15.996 Re_\omega^{0.4806} Pr^{5.5} \qquad He \qquad (27)$$

$$A_0 = 101.9 \quad \& \quad 7.9 < Re_\omega < 118.4$$

$$\overline{Nu} = 1.296 Re_\omega^{0.6584} Pr^{5.5} \qquad CO_2 \qquad (28)$$

$$A_0 = 101.9 \ \& \ 92.9 < Re_\omega < 1335.9$$

The average value of friction coefficient in the heater for carbon dioxide and helium are calculated from eq. 29-3۰. The rate of change in the friction coefficient for the mentioned fluids versus kinetic Reynolds number in shown in fig. 7.

$$\bar{C}_f = 12.737 \times A_0 \times Re_\omega^{-0.614} \qquad He \qquad (29)$$

$$A_0 = 101.91 \ \& \quad 8 < Re_\omega < 118$$

$$\bar{C}_f = 2.9941 \times A_0 \times Re_\omega^{-0.312} \qquad CO_2 \qquad (30)$$

$$A_0 = 101.91 \ \& \quad 92 < Re_\omega < 1684$$

[DOI: 10.22068/ase.2020.547]

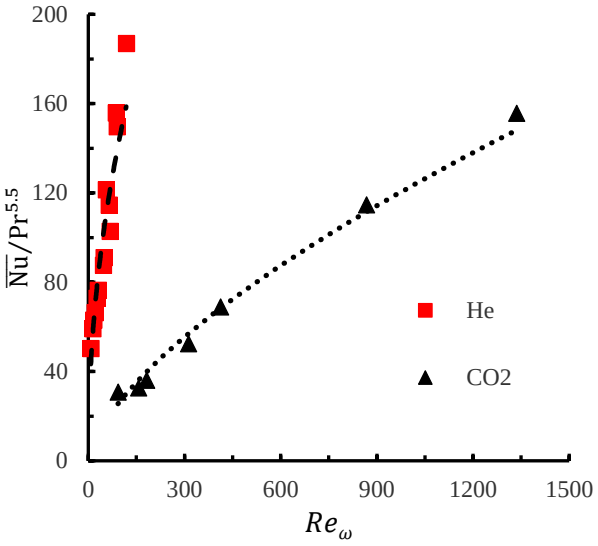

Figure 6: average heater Nusselt number changes for helium and carbon dioxide

The average Nusselt number inside the cooler section for both carbon dioxide and helium is shown in fig.8 in terms of Prandtl and kinetic Reynolds numbers. The average Nusselt number inside the cooler of the Stirling engine for both mentioned fluids can be calculated from eq. 30-31. The overall heat transfer inside the cooler can be found using average Nusselt number and geometry of the cooler.

$$\overline{Nu} = 8.24\, Re_w^{0.52} Pr^2 \qquad He \qquad (۳۰)$$

$$A_0 = 473.8 \;\; \& \;\; 2.9 < Re_\omega < 24.3$$

$$\overline{Nu} = 4.52\, Re_w^{0.65} Pr^2 \qquad CO_2 \qquad (۳۱)$$

$$A_0 = 473.8 \;\; \& \;\; 100.6 < Re_\omega < 374.7$$

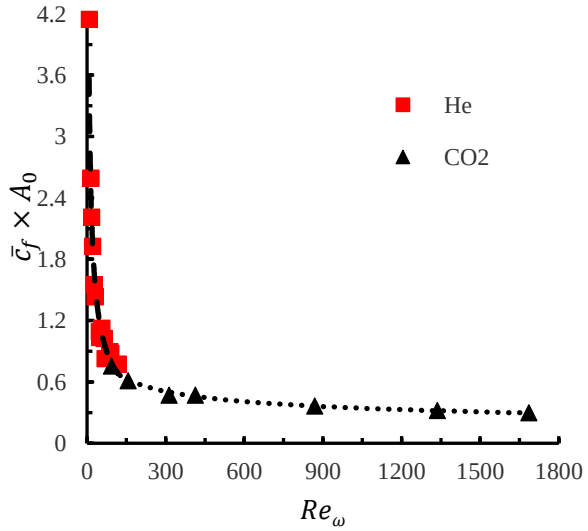

Figure 7: Variation of heater's average coefficient of friction for both helium and carbon dioxide.

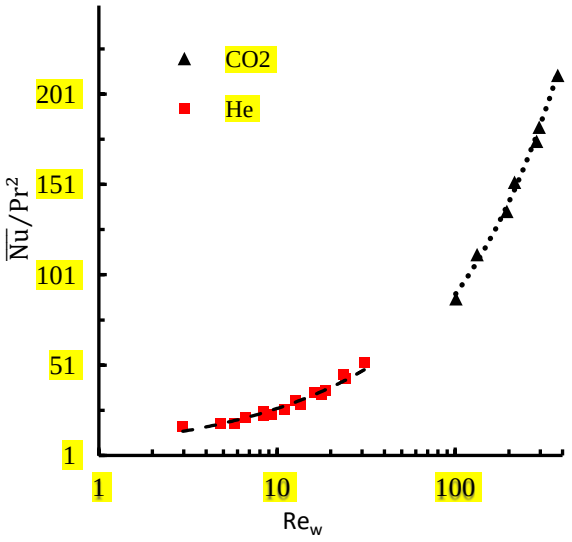

Figure 8: extracting a correlation for average Nusselt number in a cooler with both helium and carbon dioxide as working fluids

A comparison of simulation and experimental results of the input heat effect on engine speed with helium as working fluid with 3 bars and 7 bars of charged pressure are shown in fig. 9.

From fig. 9 it can be seen that by increasing heat input rate, we can increase the engine rotational speed; and also that in high charged pressures more heat can be transferred by the working fluid than in lower engine speeds. This can be explained by the increase in gas density due to increased gas pressure.

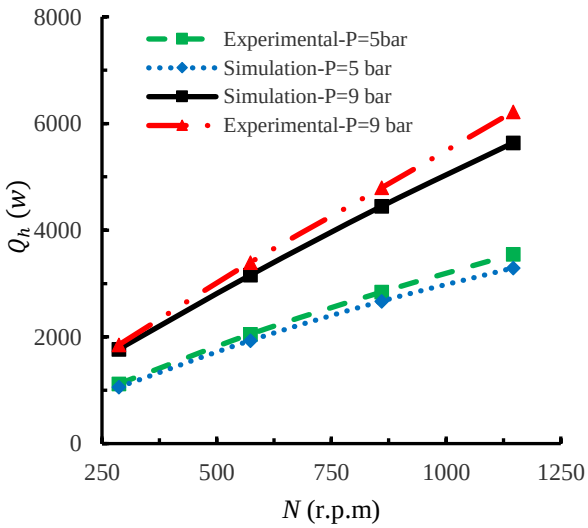

Figure 9: Rate of change of input heat against Stirling engine working speed for both helium.

In fig. 10 the relation between generated power and engine speed when running on helium as working fluid is shown experimentally. From fig. 10 one can see that by increasing engine speed, generated power will reach a maximum value from which

[DOI: 10.22068/ase.2020.547]

onwards, as the engine speeds increases further the generated power will decrease. Also it is shown by increasing the charge pressure, the occurrence zone of maximum power will shift towards higher engine speeds.

We understand for each specific engine speed, there exists a single optimum maximum power value, which declines in value if the engine speed increases beyond a certain specific speed; this can be explained by rapid increase in frictional forces as the engine cycles faster. For instances, it was seen when we tried to increase the engine speed beyond 810 rpm for helium at 3 bars; the frictional forces were so great, the extra generated power was totally cancelled out by frictional forces, plus it even declined further as friction forces took advantage even more. But when we increased the charge pressure to 5 bars, the optimum generated power occurred near 800 rpm; and when we further increased the charge pressure to 9 bars, the optimum power occurred at around 1000 rpm zone. Similar experiments have been held for carbon dioxide as well. From the simulation results of the cooler and heater, one can determine heat input/output to and from the engine, which is useful data for thermal analysis of the engine. Knowing the Nusselt number and the conduction coefficient of the fluid, one can find the convection coefficient along with total heat transfer value.

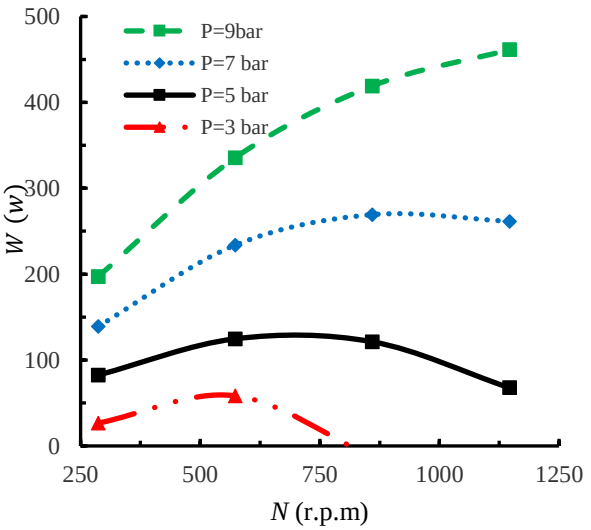

Figure 10: Rate of changes in generated power at different engine speeds for helium as working fluid

The results of a thermal analysis conducted on a Stirling engine is shown in table. 6, in order to do so, we calculated input and output heat to and from the engine, power generated and its efficiency for helium and carbon dioxide working fluids with 3-9 bars pressure and 30-120 rad/s engine speeds.

In table 6 data presented for helium at 5-9 bars was measured experimentally. But the rest of the data was extracted from simulation results. We conducted multi objective optimization on the ST-500 Stirling engine at 5-9bars of pressure, 286-1146rpm engine speed, for helium and carbon dioxide working fluids. Efficiency, generated power and total losses in cooler and heater were chosen as target functions. Our aim was to maximize efficiency and generated power while keeping pressure losses as low as possible. In order to simulate this process with three target functions and two variables. Namely pressure and engine speed; it was necessary to simulate four operational points in the engine. These four points are detailed in table 7 for helium (rows 1-4) and carbon dioxide (rows 5-8).

In fig.11 the variation of target functions, as individual, and their overall effect, considering DOE method was examined. The significant factor was one for all three target parameters. It was shown that the optimum operation point for helium as working fluid, occurs at about 9bars and 425 rpm. The total target function for this point was D=0.6962. The efficiency, generated power and pressure loss for this point were 10.65 and 239.8watt and 9987.4Pa respectively. Also the value of the separate functions mentioned were 0.9475, 0.4371 and 0.8148 respectively. (I1, I2, I3 were significant factors for efficiency, generated power and pressure losses) Also the separate target functions for efficiency, generated power and pressure losses were 9.34, 357.2 watt and 25269.5 Pa respectively.

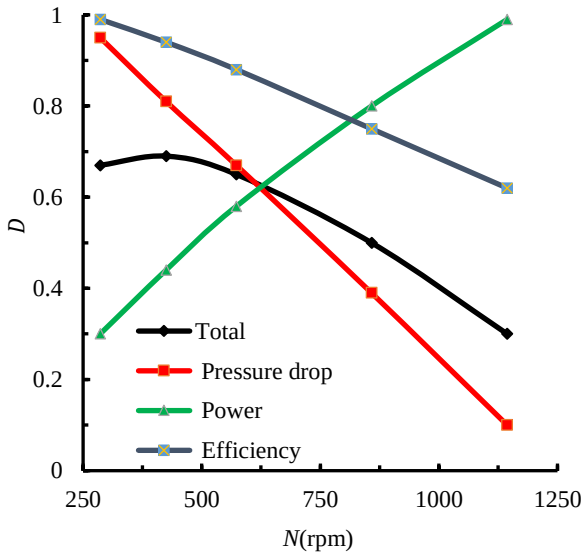

Figure 11: overall and individual target function for ST500 engine, in the range of 5-9 bars of pressure and 286-1146 rpm engine speed for heium with the condition that : ($I_1 = I_2 = I_3 = 1$)

[DOI: 10.22068/ase.2020.547]

Table 6: Thermal balance (input/output heat and generated power) in 3-9 bars range for engine speeds of 30-120 rad/s for helium

Item	Fluid	Pressure (bar)	N(r.p.m)	Q_h (W)	Q_l (W)	Work(W)	Efficiency (%)
1	He	3	286	653.6	89.3	26.5	4.1
2	He	3	573	1372.9	192.4	58.4	4.3
3	He	5	286	1057.9	161.4	82.5	7.8
4	He	5	573	1930.7	351.7	124.7	6.4
5	He	5	858	2670.2	557.1	121.3	4.5
6	He	5	1146	3292.5	772.7	67.8	2.1
7	He	7	286	1551.8	246.9	139.1	8.9
8	He	7	573	2653.7	537.6	233.8	8.8
9	He	7	858	3758.2	850.2	269.3	7.2
10	He	7	1146	4822.3	1175.4	261.5	5.4
11	He	9	286	1770	344.8	197.1	11.1
12	He	9	573	3157.3	751.9	335.5	10.6
13	He	9	858	4447.7	1182.7	419.1	9.4
14	He	9	1146	5636.2	1627.6	461.3	8.2
15	CO_2	3	286	421.6	105.7	23.9	5.7
16	CO_2	3	573	605.5	230.4	2.2	0.4
17	CO_2	5	286	998.5	199.1	77.7	7.8
18	CO_2	5	573	1473.2	402.1	52.8	3.6
19	CO_2	7	286	1803.3	200.4	160.2	8.9
20	CO_2	7	573	3625.2	404.5	142.5	4.1
21	CO_2	9	286	2571.3	431.4	212.5	8.3
22	CO_2	9	573	4544.1	901.2	262.7	5.8
23	CO_2	9	858	6337.5	1456.3	21.8	0.4

Table 7: 5 required simulation data of the four points for optimization

Item	Fluid	Pressure (bar)	Engine speed (r.p.m)	Efficiency(%)	Power (W)	Pressure drop (Pa)
1	He	5	286	7.79	82.5	3434.9
2	He	9	286	11.13	197.1	4430.3
3	He	5	1146	2.05	67.8	25241.9
4	He	9	1146	8.18	461.3	38817.9
5	CO_2	5	286	7.78	77.7	11277.4
6	CO_2	9	286	8.3	212.5	17579.4
7	CO_2	5	573	3.6	52.8	25520.2
8	CO_2	9	573	5.8	262.5	70532.3

[DOI: 10.22068/ase.2020.547]

*Corresponding Author
Email Address: keshavarz@kntu.ac.ir
http:// tlx.doi.org/10.22068/ijae.10.3.3281

The results of our optimization for the Stirling engine using different setups of significance factor, and helium as the working fluid is presented in table 8. As a reminder, the significance factor could range from 1-10. In table 8, we covered all possible extreme-end conditions of this factor, in order to clearly show the important effects caused by each factor.

These findings are highlighted:

- Optimum working pressure for helium at all points was 9bars
- If the significance factor was considered equal, optimum engine speed would be 424.9 rpm. Also if one were to raise the significance factor of efficiency to 5-10 rang whilst keeping others at 1; optimum engine speed would be 286rpm at 9bars pressure.

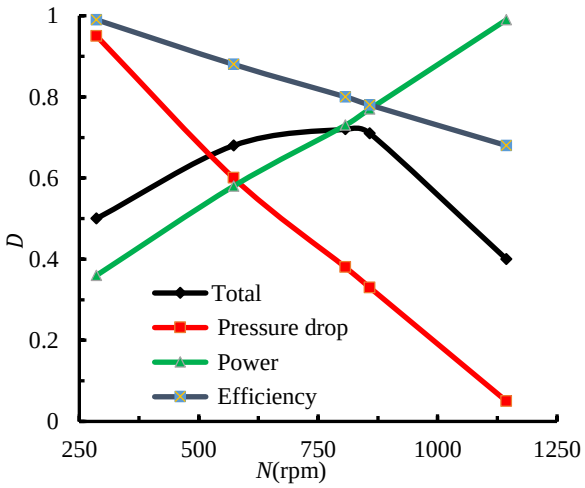

Figure 12: overall and individual target functions for ST500 engine in the range of 5-9 bars of pressure and 286-1146 rpm engine speed for heium with the condition that : ($\boldsymbol{I_1 = I_2 = 5}$ & $\boldsymbol{I_3 = 1}$)

Table 8: Optimization results for Stirling engine with helium (I1, I2 and I3 represent efficiency, generated power and pressure drop significance factor respectively)

Item	I_1	I_2	I_3	Pressure (bar)	Engine speed(r.p.m)
1	1	1	1	9	424.9
2	5	1	1	9	286
3	10	1	1	9	286
4	1	5	1	9	911.5
5	1	10	1	9	1024.4
6	1	1	5	9	286
7	1	1	10	9	286
8	1	5	5	9	485.8
9	1	5	10	9	286
10	1	10	5	9	711.6
11	1	10	10	9	494.5
12	5	1	5	9	286
13	5	1	10	9	286
14	10	1	5	9	286
15	10	1	10	9	286
16	5	5	1	9	807.2
17	5	10	1	9	989.6
18	10	5	1	9	650.8
19	10	10	1	9	920.1

- If one were to raise the significance factor for developed power to 5 and then to 10, whilst keepings others at 1, optimum engine speed would be 911.5 rpm and 1024.4 rpm respectively. This also suggests if one was to set the significance factor to something between 5 and 10 for power whilst keepings others at 1; an optimum engine speed somewhere between 911.5 rpm and 1024.4 rpm is to be expected.
- If one were to increase significance factor for pressure drop to 5 and 10, whilst keeping others at 1, optimum speed would be 286 rpm with 9 bars (again).
- If the significance factor for efficiency was set to 1 whilst the significance factor for developed power and pressure drop was set at 5 and 10; the optimum speed would be somewhere between 494.5-485.5 rpm. In this condition, as the significance factor for pressure drop grows from that of developed power, the optimum speed reduces to about 286 rpm.
- If the significance factor for developed power as set at 1 whilst significance factor for efficiency and pressure drop were set to 5 and 10; the optimum speed would be around 286 rpm.
- If the significance factor for pressure drop was set to 1 whilst significance factor for developed power and efficiency were set at 5 and 10, the optimum speed would be 807.2 and 920.1 rpm respectively. If the significance factor for power was to be increased, optimum speed would reach to about 989.6r pm. Similarly, if the significance factor for efficiency was to be increased the optimum speed would reduce to about 650.8 rpm.

[DOI: 10.22068/ase.2020.547]

The optimum operation point for helium at 9bars takes place at about 286rpm engine speed. The overall target function at this point is 0.8401. The exact values of efficiency, power and pressure loss were 18.3, 212.5w, 17579.4Pa respectively. The separate target function for efficiency, power and pressure loss were 1.00, 0.7615 and 0.7785 respectively.

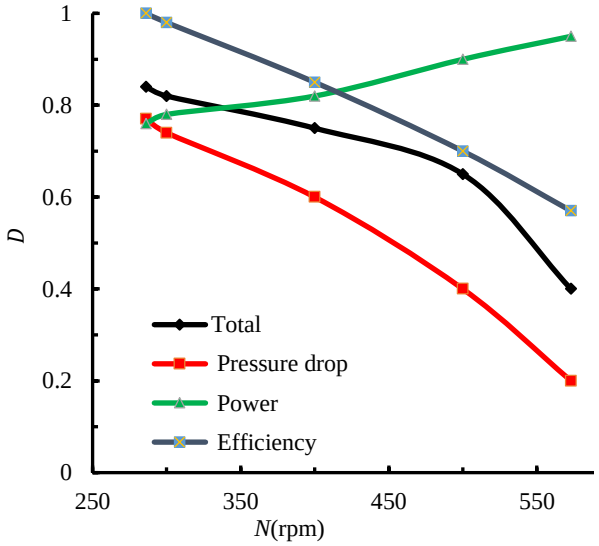

Figure 13: Overall and individual target function for st500 Stirling engine running on carbon dioxide in operational range of 5-9bars and 286-1146 rpm with significance factors of: ($\boldsymbol{I_1 = I_2 = I_3 = 1}$)

Table 9: Optimization results for Stirling engine with carbon dioxide (I_1, I_2 and I_3 represent efficiency, generated power and pressure drop significance factor respectively)

Item	I_1	I_2	I_3	Pressure (bar)	Engine speed(r.p.m)
1	1	1	1	9	286
2	5	1	1	9	286
3	10	1	1	9	286
4	1	5	1	9	291.8
5	1	10	1	9	428.1
6	1	1	5	9	286
7	1	1	10	8.1	286
8	1	5	5	9	286
9	1	5	10	9	286
10	1	10	5	9	286
11	1	10	10	9	286
12	5	1	5	9	286
13	5	1	10	9	286
14	10	1	5	9	286
15	10	1	10	9	286
16	5	5	1	9	286
17	5	10	1	9	286
18	10	5	1	9	286
19	10	10	1	9	286

By Table 9 We can arrive at these conclusions:

- Optimum working pressure for co_2, for all points were 9 bars; except when significance factor of pressure drop was 10 and the rest were set at 1.
- Optimum engine speed was 286 rpm for the cases where all three target functions had identical significance factor. If we raised the significance factor for efficiency to a 5-10 range, whilst keeping others constant; optimum operational point at 9 bars of pressure would be reached at 286 rpm engine speed.
- By increasing the significance factor for power to a 5-10 range, whilst keeping others at 1, optimum speed tends towards 291.8 and 428.1 respectively. So if we were to consider a significance factor of 7 for power (keeping others unchanged at 1), we should expect an optimum speed to be in the midrange of 291.8-428.1rpm.
- By increasing the significance factor of pressure to 5 and 10 (keeping others unchanged) the optimum engine speed occurred at about 286 rpm at 9 bars if charge pressure.
- By considering a significance factor of 1 for efficiency, and increasing the significance factors of power and pressure loss to 5 and 10; the optimum engine speed will tend towards 286 rpm.
- By considering a significance factor of 1 for power, and increasing the significance factors of efficiency and pressure drop to values of 5 and 10; the optimum engine speed will tend towards 286 rpm.

In other words, for carbon dioxide as working fluid, it is seen that optimum conditions occur at lower rpm's. The reason for this is mainly because of significant increases in friction losses due to heavier molecular weight of carbon dioxide (in comparison to helium).

It is shown in table 9 that for a Stirling engine operating on carbon dioxide at 5bars, the output

[DOI: 10.22068/ase.2020.547]

power at 286rpm is 77.7watt and as the engine speed increases to 573 rpm; the generated power declines to 52.8 watt as frictional effects take over.

6. Conclusion

Experimental tests have been conducted on the ST-500 gamma Stirling engine with helium as operating fluid at 9 and 5 bars, with engine speed of 286-1146rpm. Also the highest percentage of simulation error for heat transfer and coefficient of friction experienced was 9.34% when the simulated engine was running on co2 as working fluid. The selected engine didn't show acceptable performance with co_2 at 3 bars in any engine speed. Even at 3-9 bars range with speeds close to 858rpm, the engine either couldn't overpower frictional losses or the generated power was just too small to perform.

Three-objective optimization was conducted with target functions of maximum efficiency and power along with minimal pressure losses in the heat exchangers. Pressure and engine speed were considered as optimization variables for helium and co_2. The results indicated that for the ST-500 engine, helium showed more working potential in higher engine speeds than co_2. Considering similar significance factor for efficiency, power and pressure losses; optimum operation point at 9 bars was achieved at 424.9 rpm for helium and 286 rpm for co_2. If we set the significance factor for helium to 5 and 10 for power (1 for efficiency and pressure loss), the optimum engine speed would be 911.5 and 1024.4 rpm respectively. If we considered the significance factor as 1 for efficiency and increase it to 5 and 10 for power and pressure loss; optimum speed will occur in the 494.5-485.5 rpm range. In this condition, the greater the pressure loss's significance factor versus the generated power's significant factor, the optimum point will shift towards 286 rpm.

However, it was shown that for co_2, if we were to increase generated power's significance factor to 5 and 10 for (maintaining significance factor of 1 for efficiency and pressure loss) the optimum performance will occur at 291.8 and 428.1 rpm respectively. Therefore, one can presume for a significance factor of 7 for power, whilst maintaining that of others at 1, the optimum speed would be experienced somewhere between 291.8 and 428.1rpm.

For most cases investigated with an engine running on co_2, optimized pressure was seen to be 9 bars with a speed of 286 rpm. This is mainly because of heavier molecular weight of co_2 in comparison to helium, giving co_2 a potential operational conditions at lower engine speeds.

References

[1] Karabulut, H., Yücesu, H. S., Çınar, C., & Aksoy, F. (2009). An experimental study on the development of a β-type Stirling engine for low and moderate temperature heat sources. Applied Energy, 86(1), 68-73.

[2] Cheng, C. , Yang, H. S., & Keong, L. (2013). Theoretical and experimental study of a 300-W beta-type Stirling engine. Energy, 59, 590-599.

[3] Toghyani, S., Kasaeian, A., Hashemabadi, S. H., & Salimi, M. (2014). Multi-objective optimization of GPU3 Stirling engine using third order analysis. Energy Conversion and Management, 87, 521-529.

[4] Ahmadi, M. H., Hosseinzade, H., Sayyaadi, H., Mohammadi, A. H., & Kimiaghalam, F. (2013). Application of the multi-objective optimization method for designing a powered Stirling heat engine: design with maximized power, thermal efficiency and minimized pressure loss. Renewable Energy, 60, 313-322.

[5] Alfarawi, S., Al-Dadah, R., & Mahmoud, S. (2016). Enhanced thermodynamic modelling of a gamma-type Stirling engine. Applied Thermal Engineering, 106, 1380-1390.

[DOI: 10.22068/ase.2020.547]

[6] Saberinejad, H., Keshavarz, A., Bastami, M., & Payandehdoost, M. (2017). A new approach for Modeling and Evaluation of efficiency and power generation in Sterling engine; Analytical study. International Journal of Automotive Engineering, 7(1), 2325-2331.

[7] Ye, W., Yang, P., & Liu, Y. (2018). Multi-objective thermodynamic optimization of a free piston Stirling engine using response surface methodology. Energy Conversion and Management, 176, 147-163.

[8] Ahmed, F., Hulin, H., & Khan, A. M. (2019). Numerical modeling and optimization of beta-type Stirling engine. Applied Thermal Engineering, 149, 385-400.

[9] Saberinejad, H., & Keshavarz, A. (2016). Reciprocating turbulent flow heat transfer enhancement within a porous medium embedded in a circular tube. Applied Thermal Engineering, 102, 1355-1365.

[10] Holman, J., & Fürst, J. (2007) NUMERICAL SOLUTION OF COMPRESSIBLE TURBULENT FLOWS USING EARSM MODEL, Colloquium Fliud Dynamics, Prague,

[11] Versteeg. H. K, Malalasekera. W, (1995) "An introduction to computational fluid dynamics, The finite volume method", Longman Scientific & Technical Pub.

[12] Azmoodeh, M., Keshavarz valian, A., Saberi Nejad, H., Batooei, A. (2015). Numerical analysis of heat transfer in turbulent reciprocating flow in Stirling engine heat exchanger. Journal of Solid and Fluid Mechanics, 5(4), 187-200. (in Persian)

[13] Dehghan A, Keshavarz Valian A, batooei A, Saberinejad H. (2018) Numerical investigation of reciprocating flow in a shell and tube heat exchanger used as a cooler in gamma Stirling engine. Modares Mechanical Engineering. 17 (10) :359-366 (in Persian)

[14] H. Saberinejad, A. Hashiehbaf, and E. Afrasiabian, 2010 "A study of various numerical turbulence modeling methods in boundary layer excitation of a square ribbed channel," World Academy of Science, Engineering and Technology, vol. 71, pp. 338-344.

[15] T. Zhao and P. Cheng, (1996) "Experimental studies on the onset of turbulence and frictional losses in an oscillatory turbulent pipe flow," Int. J. Heat and Fluid Flow, vol. 17, pp. 356-362,

[16] T. Zhao and p. Cheng, (1996) "The friction coefficient of a fully developed laminar reciprocating flow in a circular pipe," Int. J. Heat and Fluid Flow,, vol. 17, pp. 167-172.

[17] S.M. Yang, W.Q. Tao, Heat Transfer, fourth ed., Higher Education Press, Beijing, 2006. pp. 246–270

[18] M. Kanzaka, M. Iwabuchi, (1992) Study on heat transfer of heat exchangers in the Stirling engine-heat transfer in a heated tube under the periodically reversing flow condition, JSME Int. J. 35 641–646.

[19] T. Zhao, P. Cheng, (1996) Oscillatory heat transfer in a pipe subjected to a laminar reciprocating flow, ASME J. Heat Transfer 11

[DOI: 10.22068/ase.2020.547]